Evidence of Cobalt-Vacancy Complexes in $Zn_{1-x}Co_xO$ Dilute Magnetic Semiconductors

G. Ciatto,[1,*] A. Di Trolio,[2] E. Fonda,[1] P. Alippi,[3] A. M. Testa,[3] and A. Amore Bonapasta[3]

[1]*Synchrotron SOLEIL, L'Orme des Merisiers, Saint-Aubin, BP48, 91192 Gif-sur-Yvette Cedex, France*
[2]*CNR–Istituto dei Sistemi Complessi, Via Salaria km. 29,300 I-00016 Monterotondo Stazione, Italy*
[3]*CNR–Istituto di Struttura della Materia, Via Salaria km. 29,300 I-00016 Monterotondo Stazione, Italy*

(Received 22 January 2011; revised manuscript received 13 July 2011; published 16 September 2011)

We investigate the local structure of ferromagnetic $Zn_{1-x}Co_xO$ epilayers by coupling polarization-dependent x-ray absorption spectroscopy and *ab initio* calculations of selected defect structures. We give clear evidence of the presence of oxygen vacancies, located close to the Co atoms in a specific complex configuration. We also establish the upper concentration limit of metallic parasitic nanophases and their contribution to magnetism. Our results lead to the conclusion that oxygen vacancies play an important role in originating the high temperature ferromagnetism of $Zn_{1-x}Co_xO$.

DOI: 10.1103/PhysRevLett.107.127206 PACS numbers: 75.50.Pp, 61.05.cj, 71.55.Gs, 85.75.−d

The field of dilute magnetic semiconductors has gained increasing interest in the past decade both for the potential technological applications in spintronic devices [1], in which semiconducting and magnetic properties are combined, and from a fundamental viewpoint due to the controversial mechanisms which are at the basis of ferromagnetic ordering in these materials. Compounds based on ZnO ($Zn_{1-x}Co_xO$ and $Zn_{1-x}Mn_xO$) are especially appealing since, contrary to GaMnAs and InMnAs, they exhibit ferromagnetism (FM) at room temperature (RT) [2,3] and have low toxicity. Despite this great potential, the understanding of RT FM in dilute ferromagnetic oxides (DFO) is far from being achieved, since the established theory of carrier-mediated magnetism [4] does not apply to the case of DFOs, where a correlation between carriers and magnetism is not evident [5]. Experimental and theoretical studies have attributed RT FM in these systems to a variety of origins including intrinsic defects [6], nonhomogeneity of the dopant spatial distribution [7], hydrogen contamination [8], or the presence of secondary phases [9] such as small Co nanoclusters. Moreover, RT FM is highly dependent upon the sample preparation and growth conditions to such an extent that some groups have even suggested that in high-quality materials FM should not be observed at all [10].

Several recent studies have focused on the role of oxygen vacancies (V_O) in the generation of RT FM: as a matter of fact, oxygen-deficient growth and annealing in vacuum produce FM [11], while annealing in oxygen reduces it [12]. At the same time, RT FM in DFOs can be accounted for by Heisenberg models or models based on spin split impurity bands involving intrinsic defects [13,14]. In this regard, while V_O are generally represented as rather deep donors [15], previous [14] and present theoretical results indicate that Co-V_O complexes in a $Zn_{1-x}Co_xO$ alloy generate electronic states close to the conduction band which could play a role in RT FM. This alloy represents therefore an interesting test bed for experimental verification of possible effects of V_O on the magnetic properties in DFOs. However, a convincing experimental demonstration of the existence of V_O in $Zn_{1-x}Co_xO$ is still missing. Several groups have tried to address this issue using x-ray absorption fine structure spectroscopy (XAFS) at the absorption edges of the constituent elements; some of them attributed certain spectral features observed at the oxygen K edge to V_O, but without providing any quantitative justification [16], while others suggested the presence of V_O in the second atomic shell of Co impurities on the basis of very tiny differences in the x-ray absorption near edge structure (XANES) of as-grown and annealed samples [17]. Hsu *et al.* [18] associated a preedge feature observed in the Zn K-edge XANES of Ar/H_2-annealed samples to the formation of V_O, but they were only able to simulate it by assuming an enormous and nonrealistic vacancy concentration. Finally, Shi *et al.* [19] excluded the presence of V_O in nonferromagnetic samples.

Rather surprisingly, up to now no group has exploited the polarization dependence of K-edge XANES to study the formation of V_O in dilute ferromagnetic oxides. In the few cases where angular dependent XANES and linear dichroism experiments were performed on $Zn_{1-x}Co_xO$, either the authors dealt with nonferromagnetic samples [10] or they did not simulate XANES spectra in the presence of V_O [20]. In this Letter, we couple angle-dependent Co K-edge XAFS analysis with state-of-the-art density functional theory (DFT) calculations of V_O-containing structures and demonstrate the existence of V_O in FM $Zn_{1-x}Co_xO$ alloys in addition to quantifying the upper concentration limit of Co metallic nanophases possibly present in the samples. Moreover, we show that V_O are preferentially located close to the Co impurities with the impurity-vacancy direction aligned along the c axis of the wurtzite lattice (Co-$V_{O\|c}$).

We studied three 600-nm-thick $Zn_{1-x}Co_xO$ epilayers ($x = 0.02$, 0.04, and 0.06) deposited on $Al_2O_3(0001)$ substrates by pulsed laser deposition. The growth temperature

 © 2011 American Physical Society

was 773 K [21]. A piece of the $x = 0.04$ sample was subsequently annealed in oxygen, following the same procedure as Han *et al.* [12]; this piece will be termed $x = 0.04(a)$ henceforth. RT magnetization versus field (H) measurements performed by means of a vibrating sample magnetometer [Fig. 1(a)] show a clear ferromagnetic behavior for all samples, with particularly high values in saturation magnetization for the $x = 0.04$ sample (about 0.44 μ_B/Co). X-ray diffraction (XRD) data [Fig. 1(b)] indicate the presence of the wurtzite structure with negligible contribution from secondary phases which testify to the high structural quality of our samples.

Angle-dependent Co K-edge XANES measurements were performed at the SAMBA beam line at the SOLEIL synchrotron radiation facility in fluorescence detection mode. We measured the samples at near-grazing incidence conditions (incidence angle $\alpha = 1°$) with the electric field vector (E) $\parallel c$, at near-normal incidence ($\alpha = 89°$) with $E \perp c$ and at the angle ($\alpha \approx 55°$) which averages out polarization effects in hexagonal crystals (the magic angle [22]). Figure 2 shows Co K-edge XANES taken on all samples with $E \parallel c$ (the four spectra at the bottom): one can clearly see the disappearance of the valley between features 1 and 2 in the spectrum of the untreated $x = 0.04$ sample compared to the $x = 0.02$ and 0.06 ones. Moreover, the amplitude of feature 3 is smaller in the untreated $x = 0.04$ sample. We checked that these changes are not due to poorer crystallinity in the $x = 0.04$ sample (see the Supplemental Material [21]). Instead, rather surprisingly, measuring in the $E \perp c$ and magic angle conditions, only minor changes between the experimental spectra of the samples are observed (not shown); in particular, the spectra taken at the magic angle are similar to those of the various works reported in the literature [9,17,19,23].

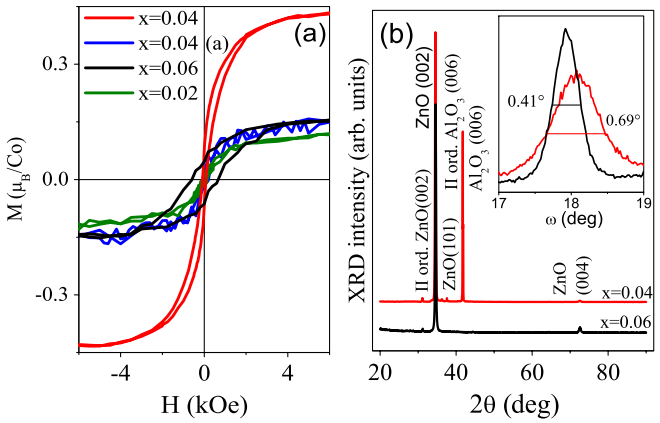

FIG. 1 (color online). (a) Hysteresis cycle for all epilayers (substrate signal has been subtracted); 0.04(a) indicates annealed in oxygen. (b) XRD θ-2θ scans performed on the $x = 0.04$ and $x = 0.06$ samples (the latter was grown with the c axis misaligned by $<1°$ with respect to the substrate) [21]. Inset: ω scan performed at the epilayer 002 peak.

We point out here that for the wurtzite group and K-absorption edges, due to the directionality of the p_x, p_y, and p_z components of the final state, with $E \parallel c$ XANES is sensitive to variations of the electronic density along the c axis, while for $E \perp c$ variations in the perpendicular components are enhanced [22]. This led us to postulate that our experimental results could be explained by a defective local configuration around the Co atoms which differs from a pure substitutional one by a modification of the electronic charge distribution along the c direction. Employing spin-polarized DFT methods [21] using the Hubbard correction [24] within the projector augmented wave method implemented in VASP [25], we calculated several defect structures, including V_O, Co-$V_{O\|c}$ complexes, Co pairs, and Co clusters. The relaxed interatomic distances calculated in this way were given as an input to the FDMNES code [26] to simulate the Co K-edge XANES in a full multiple scattering (FMS) approach.

One of the stable V_O configurations we found from these calculations corresponds to the complex sketched in the inset of Fig. 2: in this case the O vacancy is located in a nearest-neighbor position with respect to a Co atom and the line joining the vacancy and the Co atom is parallel to the c axis. For the resulting complex (Co-$V_{O\|c}$), we calculated a reduction in total energy of about 0.24 eV with respect to the initial state (isolated Co plus simple V_O). Such a Co-$V_{O\|c}$ binding energy can be accounted for by local relaxations around the Co atom (and related electronic structure rearrangements) which are favored by the neighboring V_O. The Co-$V_{O\|c}$ configuration is slightly lower in

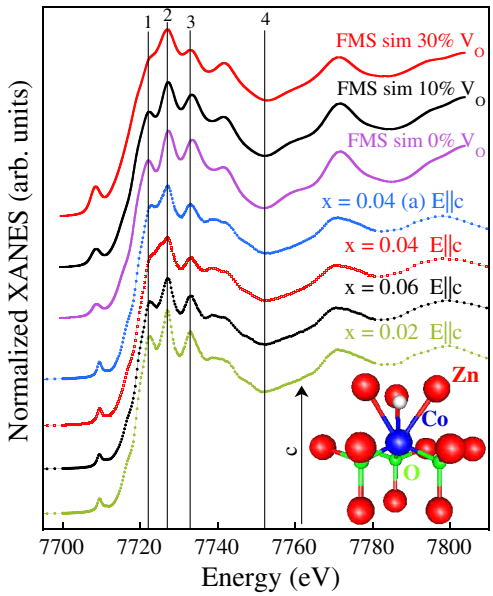

FIG. 2 (color online). Co K-edge XANES taken with $E \parallel c$ on all samples (bottom spectra) and FMS simulations (top spectra). Inset: Sketch of the Co-$V_{O\|c}$ complex used in the simulations. The V_O is represented by the white sphere.

energy with respect to configurations having the V_O in the plane perpendicular to the c axis. A fine analysis of site- and symmetry-projected density of states of these two different configurations [21] shows that such a complex anisotropy can be accounted for by a larger hybridization between Co states involving the d orbitals along the c axis and the V_O-induced states. This is also responsible for major modifications of the electronic structure with respect to substitutional Co which, as anticipated, include the appearance of empty levels close to the conduction band. In Fig. 2, we show FMS simulations at the Co K edge ($E \parallel c$) by combining the simulation for Co-$V_{O\parallel c}$ complexes with that of substitutional Co (upper two spectra, continuous line). The spectrum for the $x = 0.04$ sample is reproduced well by replacing $30 \pm 5\%$ of substitutional Co atoms by Co-$V_{O\parallel c}$ complexes, while $10 \pm 5\%$ of complexes is sufficient to simulate well the spectrum of the $x = 0.06$ sample: in fact, the higher percentage of complexes in the former simulation closes the valley between features 1 and 2 and decreases the amplitude of feature 3. The spectrum of the $x = 0.02$ sample shows the deepest valley and it is better reproduced by a simulation with no vacancies. We remark that, considering the Co concentration in our samples, the total percentage of V_O estimated from our XANES analysis is 1.2% in the $x = 0.04$ sample and 0.6% in the $x = 0.06$ one, which are reasonable values according to theoretical predictions [14]. XANES taken on the $x = 0.04(a)$ sample (Fig. 2) shows that the valley between features 1 and 2 reforms after annealing in oxygen, even if the recovery is not complete; in parallel, saturation magnetization decreases to one-third of the original value (Fig. 1): this confirms that variations in the XANES line shape and RT FM are related to the formation of V_O. In contrast, for $E \perp c$ (not shown), FMS simulations have a rather similar line shape that is very weakly dependent on the percentage of Co-$V_{O\parallel c}$ complexes implemented, in agreement with the small changes that are observed between the experimental spectra.

One group has used the maximum amplitude of the x-ray linear dichroism (XLD) signal, calculated from the difference between the $E \perp c$ and $E \parallel c$ XANES spectra to estimate the substitutional fraction of Co atoms and to evaluate the structural quality of the samples [10]. In this present work, we obtain an XLD signal equal to 47%, 46%, 32%, and 40% of the edge jump in the $x = 0.02$, 0.06, and 0.04 (untreated, annealed) samples, respectively, in agreement with previous experiments performed on high-quality samples [10,20]. However, we believe that this procedure is only semiquantitative in estimating the substitutional fraction of Co atoms; therefore, we performed a full quantitative analysis of the extended x-ray absorption fine structure (EXAFS) spectra. EXAFS $k^3\chi(k)$ spectra taken at the magic angle for all samples were extracted from the raw data using the ATHENA code [27], and are shown in the inset of Fig. 3. The body of Fig. 3 shows the Fourier

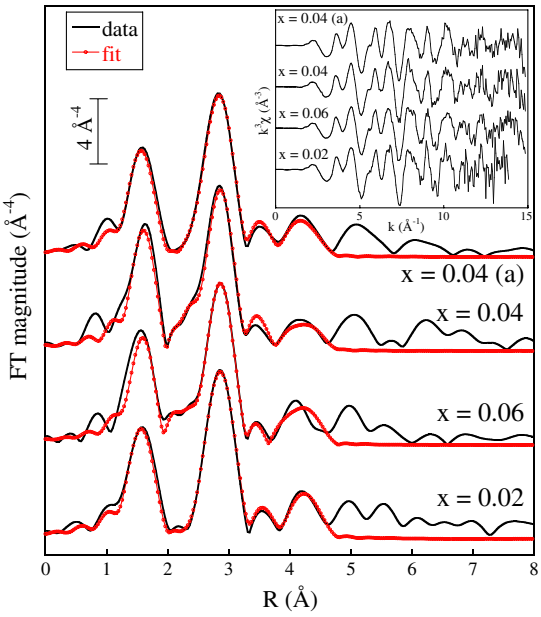

FIG. 3 (color online). Fourier transform of the EXAFS spectra (continuous line) and fits corresponding to combination of substitutional Co, metallic Co, and Co-$V_{O\parallel c}$ complexes (circle). Inset: Background-subtracted EXAFS spectra.

transform (FT) of the same spectra performed in the k range (4.8–13 Å^{-1}) (continuous line): the FT peaks at increasing radial distance represent the first few neighbor shells around the absorber. We used the same DFT-calculated model structures employed for the XANES simulations to generate EXAFS theoretical amplitudes and phase shifts via the FEFF code [28], then the theoretical XAFS signals were Fourier transformed together with the experimental ones and fits performed using the ARTEMIS code [27].

The possibility of using the accurate values calculated by DFT for the atomic positions and distance distribution from the absorber allowed us to minimize the number of fit variables and perform a fit weighting three different model structures: Co-$V_{O\parallel c}$ complexes (where paths are all multiplied by an amplitude reduction factor y), metallic Co (weighted by w), and substitutional Co (weighted by $1\text{-}y\text{-}w$). The interatomic distances and Debye-Waller factors of the metallic contribution, together with the S_0^2 many body factor, were fixed to the values extracted from the analysis of experimental Co foil data, whereas the variables fitting the thermal part of the Debye-Waller factors and the differences between actual and model distances were constrained to assume the same values for the Co-$V_{O\parallel c}$ complex and Co substitutional contributions. This analysis is different from those described in several previous papers [17–19,29] where for XAFS simulations atomic positions in the model clusters were simply generated from the lattice parameters determined by crystallography. However, in the case of vacancies, where a relaxation around the defect is expected, not accounting for deviations from

TABLE I. Structural parameters extracted from the fits to the EXAFS data taken at the magic angle: Co-$V_{O\|c}$ complex fraction (y), Co metal fraction (w), 1st shell Co-O average distance ($R_{\text{Co-O}}$), 2nd shell Co-Zn average distance ($R_{\text{Co-Zn}}$), 1st shell Debye-Waller factor ($\sigma^{\text{1st shell}}$), and 2nd shell Debye-Waller factor ($\sigma^{\text{2nd shell}}$). 0.04($a$) indicates annealed in oxygen.

Sample	y (%)	w (%)	$R_{\text{Co-O}}$ (Å)	$R_{\text{Co-Zn}}$ (Å)	$\sigma^{\text{1st shell}}$ (10^3 Å^2)	$\sigma^{\text{2nd shell}}$ (10^3 Å^2)
$x = 0.06$	0 ± 21	6.4 ± 2.8	1.968 ± 0.010	3.222 ± 0.012	3.3 ± 0.9	7.2 ± 0.8
$x = 0.04$	18 ± 14	3.7 ± 2.1	1.980 ± 0.006	3.219 ± 0.009	2.6 ± 0.6	6.8 ± 0.5
$x = 0.04(a)$	9 ± 14	0.3 ± 1.9	1.971 ± 0.007	3.219 ± 0.007	3.3 ± 0.6	7.0 ± 0.5
$x = 0.02$	0 ± 14	0.1 ± 1.8	1.979 ± 0.006	3.227 ± 0.007	3.2 ± 0.6	7.0 ± 0.5

the ideal atomic crystallographic positions would lead to erroneous results.

The fits performed following this procedure are superimposed on the data in Fig. 3 (circles). The main structural parameters extracted from the fit are reported in Table I. The y values extracted from the EXAFS data are in agreement with those derived from the XANES simulations, even if the error bars are relatively large due to the lower sensitivity of EXAFS to the presence of Co-$V_{O\|c}$ complexes with respect to XANES. EXAFS analysis gives, on the other hand, very small error bars when measuring the percentage of Co atoms involved in metallic parasitic nanophases (with respect to the total Co atoms): we obtain the highest value ($w = 6.4\%$) for the $x = 0.06$ sample.

The estimation (from the 1σ uncertainties of the fit) of the maximum possible value for the concentration of Co metallic nanophases allows us to make quantitative considerations on the origin of RT FM. Considering the Co atomic magnetic moment (1.6–1.7 μ_B) and the dimension of the samples, even if the spins in the Co metallic nanophases were completely ferromagnetically aligned, this would still only be able to account for 28% and 13% of the observed magnetism in the $x = 0.06$ and $x = 0.04$ samples, respectively. This makes clear that only considering the presence of small Co nanoclusters, invisible to XRD, cannot account for RT FM in our samples and a second mechanism is needed to explain the phenomena. The observation of larger magnetic moments in the sample where a larger percentage of V_O are detected, along with the decrease of both magnetism and V_O concentration after annealing in oxygen, strongly suggests a V_O-related mechanism. This could be provided, for example, by split-spin impurity band models similar to that recently proposed in Ref. [13] or by the blocked superparamagnetism suggested by Pemmaraju *et al.* [14]. In both cases, a partially filled donorlike band would be required and could be realized by the concurrent presence of Co-$V_{O\|c}$ complexes and shallow donors. We point out that the higher coercivity of the $x = 0.06$ sample [Fig. 1(a)] can be due to the higher fraction of metallic Co with respect to the other samples and/or to the different size of the structurally coherent domains [20 nm vs 12 nm for the $x = 0.04$ sample, as determined from XRD, Fig. 1(b)].

In conclusion, we have provided direct evidence of the existence of cobalt-vacancy complexes in high-structural quality $Zn_{1-x}Co_xO$ epilayers; such complexes consist of an oxygen vacancy located in a nearest-neighbor position with respect to the Co atom along the c axis of the wurtzite structure. A larger percentage of these Co-$V_{O\|c}$ complexes in the sample brings about an enhancement of RT FM, indicating that they play an active role in the origin of the observed magnetic moment, in agreement with some of the most recent theoretical models of dilute ferromagnetic oxides. The strength of our approach with respect to previous works in this field resides in the exploitation of the polarization dependence of x-ray absorption spectroscopy and state-of-the-art density functional theory calculations to perform a full quantitative investigation of the local environment of Co atoms and the three-dimensional structure of the Co-$V_{O\|c}$ complex. Present results provide a significant contribution to the understanding of the origin of ferromagnetism in DFOs.

We acknowledge computational resources of CASPUR (Competitive HPC Grant 2009) and the Synchrotron SOLEIL staff for general facilities placed at our disposal. We are grateful for careful reading of the manuscript by Dr. James Ablett.

*gianluca.ciatto@synchrotron-soleil.fr

[1] H. Ohno, Science **281**, 951 (1998).
[2] P. Sharma *et al.*, Nature Mater. **2**, 673 (2003).
[3] M. Venkatesan *et al.*, Phys. Rev. Lett. **93**, 177206 (2004).
[4] T. Dietl *et al.*, Science **287**, 10 19 (2000).
[5] A. J. Behan *et al.*, Phys. Rev. Lett. **100**, 047206 (2008).
[6] D. Rubi *et al.*, Phys. Rev. B **75**, 155322 (2007).
[7] S. Kuroda *et al.*, Nature Mater. **6**, 440 (2007).
[8] S. Lee *et al.*, Appl. Phys. Lett. **94**, 212507 (2009).
[9] S. Yin *et al.*, Phys. Rev. B **73**, 224408 (2006).
[10] A. Ney *et al.*, Phys. Rev. Lett. **100**, 157201 (2008).
[11] A. Dinia *et al.*, J. Appl. Phys. **97**, 123908 (2005).
[12] X. Han *et al.*, Thin Solid Films **491**, 249 (2005).
[13] J. M. D. Coey, M. Venkatesan, and C. B. Fitzgerald, Nature Mater. **4**, 173 (2005).
[14] C. D. Pemmaraju *et al.*, Phys. Rev. B **78**, 054428 (2008).
[15] A. Janotti and C. G. Van de Walle, Rep. Prog. Phys. **72**, 126501 (2009), and references therein.
[16] S. Krishnamurthy *et al.*, J. Appl. Phys. **99**, 08M111 (2006).
[17] S. Zhang *et al.*, J. Synchrotron Radiat. **17**, 600 (2010).

[18] H. S. Hsu *et al.*, Appl. Phys. Lett. **88**, 242507 (2006).
[19] T. Shi *et al.*, Appl. Phys. Lett. **90**, 102108 (2007).
[20] A. Barla *et al.*, Phys. Rev. B **76**, 125201 (2007).
[21] See Supplemental Material at http://link.aps.org/supplemental/10.1103/PhysRevLett.107.127206 for additional details on sample growth, theoretical calculations, XRD, and simulation of crystalline misorientation.
[22] C. Brouder, J. Phys. Condens. Matter **2**, 701 (1990).
[23] T. C. Kaspar *et al.*, Phys. Rev. B **77**, 201303 (2008).
[24] S. L. Dudarev *et al.*, Phys. Rev. B **57**, 1505 (1998).
[25] G. Kresse and J. Furthmüller, Phys. Rev. B **54**, 11 169 (1996).
[26] Y. Joly, Phys. Rev. B **63**, 125120 (2001).
[27] B. Ravel and M. Newville, J. Synchrotron Radiat. **12**, 537 (2005).
[28] A. L. Ankudinov *et al.*, Phys. Rev. B **58**, 7565 (1998).
[29] G. Martinez-Criado *et al.*, Appl. Phys. Lett. **89**, 061906 (2006).